ECCOMAS Congress 2016
VII European Congress on Computational Methods in Applied Sciences and Engineering
M. Papadrakakis, V. Papadopoulos, G. Stefanou, V. Plevris (eds.)
Crete Island, Greece, 5–10 June 2016

A SEMI-IMPLICIT MICROPLAR DISCRETE-TO-CONTINUUM METHOD FOR GRANULAR MATERIALS

Kun Wang[1], **WaiChing Sun**[1]

[1]Department of Civil Engineering and Engineering Mechanics, Columbia University
614 SW Mudd, Mail Code: 4709, New York, NY 10027
e-mail: {kw2534,wsun}@columbia.edu

Keywords: Micropolar Continua, Discrete-to-Continuum, Granular Matters, Length Scale, Strain Localization.

Abstract. *A micropolar discrete-continuum coupling model is proposed to link the collectively particulate mechanical simulations at high-order representative elementary volume to field-scale boundary value problems. By incorporating high-order kinematics to the homogenization procedure, contact moment and force exerted on grain contacts are homogenized into a non-symmetric Cauchy stress and higher-order couple stress. These stress measures in return become the constitutive updates for the macroscopic finite element model for micropolar continua. Unlike the non-lcoal weighted averaging models in which the intrinsic length scale must be a prior knowledge to compute the nonlocal damage or strain measures, the proposed model introduces the physical length scale directly through the higher-order kinematics. As a result, there is no need to tune or adjust the intrinsic length scale. Furthermore, since constitutive updates are provided directly from micro-structures, there is also no need to calibrate any high-order material parameters that are difficult to infer from experiments. These salient features are demonstrated by numerical examples. The classical result from Mindlin is used as a benchmark to verify the proposed model.*

1 INTRODUCTION

A granular material is a conglomeration of interacting solid particles. Collectively, these particles may store elastic strain energy while they are bonded or in contact with each other [1, 2], and dissipate energy due to grain sliding, rotation and fracture or fragmentation. The applications and handling of granular materials are central to numerous industries, such as geotechnical engineering, pharmaceutical and food processing. When the particles of the granular assembly are neither bonded nor subjected to confining pressure, granular flow may occur [3]. On the other hand, the collective macroscopic responses of these interacting particles may exhibit traits that are similar to those of a solid continuum [4, 5, 6, 1, 7].

In the past decades, theoretical and computational models designed to model granular materials in solid-like state have achieved great success. In particular, the critical state theory has been widely used as a tool to predict granular materials in both dense and loose states. Nevertheless, the prediction of constitutive responses of granular materials after the onset of strain localization remains a challenging task. One ongoing problems is that numerical methods, such as finite element or finite volume method requires the usage of macroscopic elasto-plastic constitutive law to approximate nonlinear responses with incremental updates. Without proper the so-called regularization limiter, the incremental numerical solution may exhibit spurious dependence on the mesh size when material bifurcation described in Rudnicki and Rice [8] occurs. In additional to introduce rate dependence in the constitutive responses, one possible remedy is to incorporate higher-order kinematics into the constitutive laws [9, 10, 11]. One example of the higher-order theory is the Cosserat theory originated by the Cosserat brothers in their treatise. [12]. The Cosserat theory has been re-discovered and studied by researchers that model granular continua with micropolar kinematics. A micropolar continuum is different than the classical Cauchy-Boltzmann continuum in the sense that material points are associated with microstructures that have orientations characterized by micro-rotation [12, 13]. This additional degree of freedom allows characteristic length or physical length scale to be introduced into the micropolar constitutive law and hence can be used as a mean to resolve the mesh sensitivity issue and captured the material size effects [14, 15, 16].

Nevertheless, developing phenomenological constitutive laws for micropolar continua is not a trivial task. This difficulty is not only due to the increased complexity of the higher-order constitutive laws, but also the extra burden to identify material parameters corresponding to the micropolar effect. While it is true that the pathological mesh dependence at the post-bifurcation regime can be resolved by explicitly modeling the interactions among grains with discrete element simulations, such an approach is not feasible for field-scale problem where large amount of particles are involved.

The purpose of this study is to propose a new multi-scale model that combines the strengths of the detailed grain-scale discrete simulations and the efficient high-order continuum-based finite element methods. The offspring discrete-continuum model able to (1) establish information exchange paths that prescribe higher order deformation (curvature) on DEM representative volume elements (RVEs) and extract higher order stress (couple stress) from RVEs, (2) naturally incorporate material length scale (related to particle size) into the multiscale model and thus improves the performance on capturing the material size effect in poly-disperse granular materials, (3) provide the physical underpinning from DEM simulations, and (4) resolve the problems associated with the mesh sensitivity when strain localization occurs.

As for notations and symbols, bold-faced letters denote tensors; the symbol '$\cdot$' denotes a single contraction of adjacent indices of two tensors (e.g. $\boldsymbol{a} \cdot \boldsymbol{b} = a_i b_i$ or $\boldsymbol{c} \cdot \boldsymbol{d} = c_{ij} d_{jk}$); the

symbol ':' denotes a double contraction of adjacent indices of tensor of rank two or higher (e.g. $\boldsymbol{C} : \boldsymbol{\epsilon}^e = C_{ijkl}\epsilon^e_{kl}$); the symbol '$\otimes$' denotes a juxtaposition of two vectors (e.g. $\boldsymbol{a} \otimes \boldsymbol{b} = a_i b_j$) or two symmetric second order tensors (e.g. $(\boldsymbol{\alpha} \otimes \boldsymbol{\beta}) = \alpha_{ij}\beta_{kl}$). As for sign conventions, we consider the direction of the tensile stress and dilative pressure as positive. We impose a superscript $(\cdot)^{\text{DEM}}$ on a variable to emphasize that such variable is inferred from DEM.

2 THEORETICAL BASIS FOR MICROPOLAR DISCRETE-CONTINUUM MODEL

Previous work on hierarchical DEM-FEM coupling models have been mainly focused on establishing coupling between discrete element simulations and Cauchy-type-continuum finite element analysis via first-order homogenization procedure [17, 6, 18, 19]. This first order homogenization is, nevertheless, only valid if the separation of scales exists [20, 21]. A separation of scales means that the characteristic length of macroscale problem l_{macro}, the size of RVEs l_{meso} and particle size l_{micro} fulfills the following inequality, i.e.

$$l_{micro} \ll l_{meso} \ll l_{macro}. \tag{1}$$

However, there are situations (e.g. presence of defects, inclusions, crack tips, dislocation) in which the meso-scale characteristic length l_{meso} is of comparable size of the macroscopic counterpart l_{marco}. In those cases, it is important to properly reflect the size effect in the homogenization procedure.

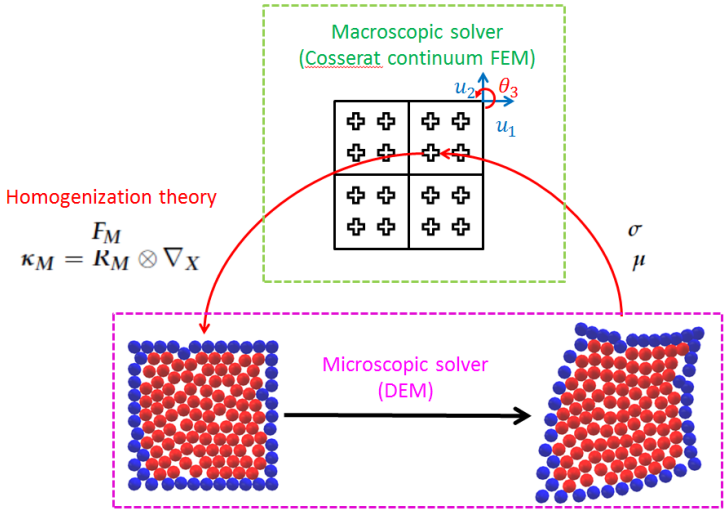

Figure 1: Multiscale discrete-micropolar continuum model

This can be done by using a high-order homogenization procedure to incorporate the size effect. The higher-order discrete-continuum coupling model proposed in this paper requires three building blocks (as shown in Fig.1): (1) the macroscopic finite element solver that provides incremental kinematic updates to the DEM solver, (2) the second order homogenization scheme that acts as an interface between the DEM and FEM solvers by converting macroscopic strain measures into constraints for RVE and up-scaling stress measures from the RVE to the integration points of the FEM solver and, (3) the DEM solver that calculate the first- and high-order stress based on the force and moment exerted on the grain contacts. To provide a proof of concepts, we have implemented a 2D micropolar DEM-FEM model for small strain problems. The following sections provide a brief outline of the the key ingredients of the numerical model, in

particular the infinitesimal micropolar theroy in 2D [22] and the second order homogenization theory [23].

2.1 2D small strain micropolar balance principle for macroscopic problems

Here we limit our attention on a prototype model that assumes the strain is infinitesimal and under plane strain condition. Recall that the kinematics of the micropolar continua can be defined by two sets of kinematic degrees of freedom that describe the changes of the position and orientation, e.g. The Cosserat strain $\boldsymbol{\gamma}$ that takes account of the higher-order kinematics is defined as a function of both the deformation gradient $u_{i,j}$ and the curvature tensor $\boldsymbol{\kappa}$, i.e.,

$$\begin{aligned}\gamma_{ij} &= u_{i,j} - \epsilon_{ijk}\theta_k \\ &= e_{ij} + w_{ij} - \epsilon_{ijk}\theta_k \\ &= e_{ij} - \epsilon_{ijk}(\theta_k - \omega_k)\end{aligned} \tag{2}$$

$$\kappa_{ij} = \theta_{i,j} \tag{3}$$

where $e_{ij} = \frac{1}{2}(u_{i,j} + u_{j,i})$ and $w_{ij} = \frac{1}{2}(u_{i,j} - u_{j,i})$ are the components of the infinitesimal strain and infinitesimal rotation tensors. ϵ_{ijk} is the component of the Levi-Civita tensor $\overset{3}{\boldsymbol{E}}$. ω_k is the axial vector of the skew-symmetric infinitesimal rotation tensor w_{ij}.

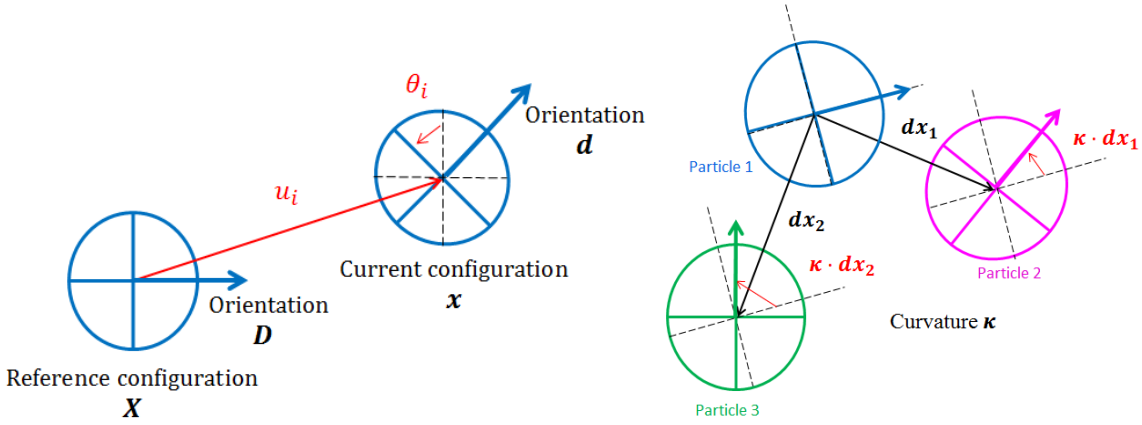

Figure 2: Micropolar kinematics. Left: displacement and rotation of a particle. Right: difference between the orientations of neighbor particles

The stress measures energy-conjugate to the micropolar strain and curvature are Cauchy stress $\boldsymbol{\sigma}$ and couple stress $\boldsymbol{\mu}$, respectively. $\boldsymbol{\mu}$ takes into the account of the moment induced by curvature. Note that, in the context of micropolar theory, the Cauchy stress $\boldsymbol{\sigma}$ no longer holds symmetry and is sometime referred as the force stress tensor [16]. Neglecting the inertia effect, the balance principle of linear and angular momentum for the static equilibrium reads,

$$\frac{\partial \sigma_{ik}}{\partial x_i} + f_k = 0, \tag{4}$$

$$\frac{\partial \mu_{ik}}{\partial x_i} + \epsilon_{imk}\sigma_{im} = 0. \tag{5}$$

For two-dimensional problem, Eq.(5) can be simplified as,

$$\frac{\partial \mu_{13}}{\partial x_1} + \frac{\partial \mu_{23}}{\partial x_2} + \sigma_{12} - \sigma_{21} = 0, \tag{6}$$

2.2 Micropolar homogenization procedure on DEM unit cells

The procedure that applies macroscopic deformation gradient $\boldsymbol{F}_M$ and curvature $\boldsymbol{\kappa}_M$ to microscopic problem is developed by Larsson and Diebels [23]. This scheme is extended to DEM RVEs based on [17]. Note the position of the center of a particle in reference configuration as $\boldsymbol{X}$ and in current configuration as $\boldsymbol{x}$. The mapping between $\boldsymbol{X}$ and $\boldsymbol{x}$ reads [23],

$$\boldsymbol{x} = \boldsymbol{F}_M \cdot \boldsymbol{X} + \frac{1}{2}((\boldsymbol{R}_M \otimes \nabla_{\boldsymbol{X}}) \cdot \boldsymbol{X}) \cdot \boldsymbol{X} + \boldsymbol{u}^f(\boldsymbol{X}), \tag{7}$$

where $\boldsymbol{u}^f(\boldsymbol{X})$ is the microstructural fluctuation of the particle center. The Hill-Mandel micro-heterogeneity condition requires that the macroscopic deformation gradient $\boldsymbol{F}_M$ is the volume average of the microscopic deformation gradient $\boldsymbol{F}$. This imposes two constraints on the DEM RVE problem: (1) the origin of the local coordinate system is set to the center of gravity of the grain assembly; (2) $\boldsymbol{u}^f(\boldsymbol{X}) = 0$ for all particles on the boundary. This corresponds to the uniform displacement boundary condition on DEM RVE.

The deformed RVEs by first-order and second-order homogenization are shown in Fig. 3. Note that in first-order the deformation is composed of extension/compression and simple shear modes, while in second-order there are additionally curvature modes.

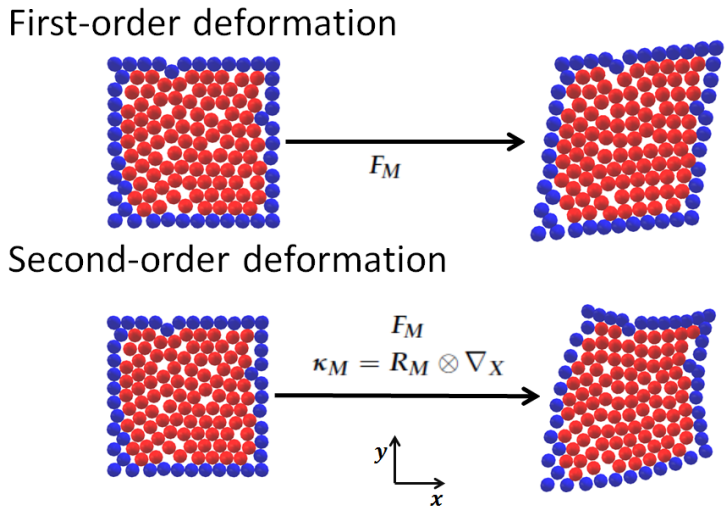

Figure 3: Deformation of DEM RVE by first-order and second-order theory

Upon deforming the RVE to a new equilibrium configuration, the macroscopic Cauchy stress is homogenized from DEM:

$$< \boldsymbol{\sigma}(\boldsymbol{x}, t) >_{\text{RVE}} = \frac{1}{\text{V}_{\text{RVE}}} \sum_{c}^{Nc} \boldsymbol{f}^c \otimes \boldsymbol{l}^c \tag{8}$$

where $\boldsymbol{f}^c$ is the contact force at the grain contact $\boldsymbol{x}^c$ and $\boldsymbol{l}^c$ is the branch vector that connects the centroids of two grains forming the contact ($\boldsymbol{x}^a$ and $\boldsymbol{x}^b$) [24, 25]. V_{RVE} is the volume of the RVE and N_c is the total number of particles in the RVE. The homogenized macroscopic couple stress can be expressed as [26]:

$$< \boldsymbol{\mu}(\boldsymbol{x}, t) >_{\text{RVE}} = \frac{1}{\text{V}_{\text{RVE}}} \sum_{c}^{Nc} (\overset{3}{\boldsymbol{E}} \cdot \boldsymbol{f}^c \otimes (\boldsymbol{x}^b \otimes (\boldsymbol{x}^c - \boldsymbol{x}^b) - \boldsymbol{x}^a \otimes (\boldsymbol{x}^c - \boldsymbol{x}^a)) + \boldsymbol{m}^c \otimes (\boldsymbol{x}^b - \boldsymbol{x}^a)) \tag{9}$$

The couple stress consists of two contributions: the eccentric contact force $\boldsymbol{f}^c$ and the contact moment $\boldsymbol{m}^c$.

3 NUMERICAL METHODS

The micropolar FEM-DEM model for plane strain problems is formulated in this section. Firstly, to construct the macroscopic boundary-value problem for micropolar continuum, consider a domain $\mathcal{B}$ with its boundary $\partial\mathcal{B}$ composed of Dirichlet boundaries (displacement $\partial\mathcal{B}_{\boldsymbol{u}}$, micro-rotation $\partial\mathcal{B}_{\boldsymbol{\theta}}$) and Von Neumann boundaries (surface traction $\partial\mathcal{B}_{\boldsymbol{t}}$, surface moment $\partial\mathcal{B}_{\boldsymbol{m}}$) satisfying

$$\begin{cases} \partial\mathcal{B} = \overline{\partial\mathcal{B}_{\boldsymbol{u}} \cup \partial\mathcal{B}_{\boldsymbol{t}}} = \overline{\partial\mathcal{B}_{\boldsymbol{\theta}} \cup \partial\mathcal{B}_{\boldsymbol{m}}} \\ \emptyset = \partial\mathcal{B}_{\boldsymbol{u}} \cap \partial\mathcal{B}_{\boldsymbol{t}} = \partial\mathcal{B}_{\boldsymbol{\theta}} \cap \partial\mathcal{B}_{\boldsymbol{m}} \end{cases} \tag{10}$$

The prescribed boundary conditions are

$$\begin{cases} \boldsymbol{u} = \overline{\boldsymbol{u}} \text{ on } \partial\mathcal{B}_{\boldsymbol{u}} \\ \boldsymbol{n}\cdot\boldsymbol{\sigma} = \overline{\boldsymbol{t}} \text{ on } \partial\mathcal{B}_{\boldsymbol{t}} \\ \boldsymbol{\theta} = \overline{\boldsymbol{\theta}} \text{ on } \partial\mathcal{B}_{\boldsymbol{\theta}} \\ \boldsymbol{n}\cdot\boldsymbol{\mu} = \overline{\boldsymbol{m}} \text{ on } \partial\mathcal{B}_{\boldsymbol{m}} \end{cases} \tag{11}$$

where $\overline{(\cdot)}$ denotes prescribed values and $\boldsymbol{n}$ is outward unit normal of surface $\partial\mathcal{B}$.

Following the standard procedures of the variational formulation, we obtain the weak form of the balance of linear momentum and angular momentum

$$\begin{aligned} G &: V_{\boldsymbol{u}} \times V_{\boldsymbol{\eta}} \to \mathbb{R} \\ G(\boldsymbol{u},\boldsymbol{\eta}) &= \int_{\mathcal{B}} \boldsymbol{\nabla}\boldsymbol{\eta} : \boldsymbol{\sigma}^{\text{DEM}} \,\mathrm{dV} - \int_{\mathcal{B}} \boldsymbol{\eta}\cdot\rho\boldsymbol{g} \,\mathrm{dV} \\ &\quad - \int_{\partial\mathcal{B}_{\boldsymbol{t}}} \boldsymbol{\eta}\cdot\bar{\boldsymbol{t}} \,\mathrm{d\Gamma} = 0 \end{aligned} \tag{12}$$

$$\begin{aligned} H &: V_{\boldsymbol{\theta}} \times V_{\boldsymbol{\psi}} \to \mathbb{R} \\ H(\boldsymbol{\theta},\boldsymbol{\psi}) &= \int_{\mathcal{B}} \boldsymbol{\nabla}\boldsymbol{\psi} : \boldsymbol{\mu}^{\text{DEM}} \,\mathrm{dV} - \int_{\mathcal{B}} \boldsymbol{\psi}\cdot\overset{3}{\boldsymbol{E}} : \boldsymbol{\sigma}^{\text{DEM}} \,\mathrm{dV} - \int_{\mathcal{B}} \boldsymbol{\psi}\cdot\rho\boldsymbol{J}\cdot\boldsymbol{c} \,\mathrm{dV} \\ &\quad - \int_{\partial\mathcal{B}_{\boldsymbol{m}}} \boldsymbol{\psi}\cdot\overline{\boldsymbol{m}} \,\mathrm{d\Gamma} = 0 \end{aligned} \tag{13}$$

The displacement and micro-rotation trial spaces for the weak form are defined as

$$V_{\boldsymbol{u}} = \{\boldsymbol{u} : \mathcal{B} \to \mathbb{R}^3 | \boldsymbol{u} \in [H^1(\mathcal{B})]^3, \boldsymbol{u}|_{\partial B_{\boldsymbol{u}}} = \overline{\boldsymbol{u}}\} \tag{14}$$

$$V_{\boldsymbol{\theta}} = \{\boldsymbol{\theta} : \mathcal{B} \to \mathbb{R}^3 | \boldsymbol{\theta} \in [H^1(\mathcal{B})]^3, \boldsymbol{\theta}|_{\partial B_{\boldsymbol{\theta}}} = \overline{\boldsymbol{\theta}}\} \tag{15}$$

and the corresponding admissible spaces of variations are defined as

$$V_{\boldsymbol{\eta}} = \{\boldsymbol{\eta} : \mathcal{B} \to \mathbb{R}^3 | \boldsymbol{\eta} \in [H^1(\mathcal{B})]^3, \boldsymbol{\eta}|_{\partial B_{\boldsymbol{u}}} = \boldsymbol{0}\} \tag{16}$$

$$V_{\psi} = \{\boldsymbol{\psi} : \mathcal{B} \to \mathbb{R}^3 | \boldsymbol{\psi} \in [H^1(\mathcal{B})]^3, \boldsymbol{\psi}|_{\partial B_{\boldsymbol{\theta}}} = \mathbf{0}\} \tag{17}$$

where H^1 denotes the Sobolev space of degree one.

The spatially discretized equations can be derived following the standard Galerkin procedure. Shape functions $\boldsymbol{N_u}(\boldsymbol{x})$ and $\boldsymbol{N_\theta}(\boldsymbol{x})$ are used for approximation of solid motion $\boldsymbol{u}$ and micro-rotation $\boldsymbol{\theta}$ respectively:

$$\begin{cases} \boldsymbol{u} = \boldsymbol{N_u}\boldsymbol{U}, \;\; \boldsymbol{\eta} = \boldsymbol{N_u}\bar{\boldsymbol{\eta}} \\ \boldsymbol{\theta} = \boldsymbol{N_\theta}\boldsymbol{\Theta}, \;\; \boldsymbol{\psi} = \boldsymbol{N_\theta}\bar{\boldsymbol{\psi}} \end{cases} \tag{18}$$

with $\boldsymbol{U}$ being the nodal displacement vector, $\boldsymbol{\Theta}$ being the nodal micro-rotation vector, and $\bar{\boldsymbol{\eta}}$, $\bar{\boldsymbol{\psi}}$ being their variations.

In the DEM-FEM implementation, a Cartesian coordinate system is adopted with axes denoted as $(\boldsymbol{x}_1, \boldsymbol{x}_2\ \boldsymbol{x}_3)$. In the two-dimensional case, we consider the cross section orthogonal to the $\boldsymbol{x}_3$-axis. A equal-order quadrilateral mixed finite element is used to interpolate the displacement and micro-rotation fields with the same standard bilinear shape functions: $\boldsymbol{N} = \boldsymbol{N_u} = \boldsymbol{N_\theta}$. For the two-dimensional problems expressed in Cartesian coordinates, the nodal generalized displacement vector contains three degree of freedoms, two for displacement and one for change of orientation, i.e.,

$$\boldsymbol{d} = [u_1 \;\; u_2 \;\; \theta_3]^{\mathrm{T}} \tag{19}$$

The generalized strain vector for 2D plane strain problems consists of the micropolar strain $\boldsymbol{\gamma}$ and the curvature $\boldsymbol{\kappa}$:

$$\boldsymbol{E} = [\gamma_{11} \;\; \gamma_{22} \;\; \gamma_{33} \;\; \gamma_{12} \;\; \gamma_{21} \;\; \kappa_{31} \;\; \kappa_{32}]^{\mathrm{T}} \tag{20}$$

The Cauchy stress $\boldsymbol{\sigma}$ and the couple stress $\boldsymbol{\mu}$ homogenized from DEM RVEs at each integration point are grouped into the generalized stress vector written as:

$$\boldsymbol{S}^{\mathrm{DEM}} = [\sigma_{11} \;\; \sigma_{22} \;\; \sigma_{33} \;\; \sigma_{12} \;\; \sigma_{21} \;\; \mu_{31} \;\; \mu_{32}]^{\mathrm{T}} \tag{21}$$

Accordingly, the element shape function matrix $\boldsymbol{N}^e$ and the generalized element B matrix $\boldsymbol{B}^e$ can be expressed as,

$$\boldsymbol{N}^e = \begin{bmatrix} N_1 & 0 & 0 & N_2 & 0 & 0 & \dots & \dots \\ 0 & N_1 & 0 & 0 & N_2 & 0 & \dots & \dots \\ 0 & 0 & N_1 & 0 & 0 & N_2 & \dots & \dots \end{bmatrix} \tag{22}$$

$$\boldsymbol{B}^e = \begin{bmatrix} \frac{\partial N_1}{x_1} & 0 & 0 & \dots & \dots \\ 0 & \frac{\partial N_1}{x_2} & 0 & \dots & \dots \\ 0 & 0 & 0 & \dots & \dots \\ \frac{\partial N_1}{x_2} & 0 & N_1 & \dots & \dots \\ 0 & \frac{\partial N_1}{x_1} & -N_1 & \dots & \dots \\ 0 & 0 & \frac{\partial N_1}{x_1} & \dots & \dots \\ 0 & 0 & \frac{\partial N_1}{x_2} & \dots & \dots \end{bmatrix} \tag{23}$$

Finally, the finite element equation for balance of linear momentum and angular momentum in domain $\mathcal{B}$ is written in a compact form as:

$$\underbrace{\int_{\mathcal{B}} \boldsymbol{B}^{\mathrm{T}} \boldsymbol{S}^{\mathrm{DEM}}\, dV}_{\boldsymbol{F}^{int}(\boldsymbol{d})} = \underbrace{\int_{\mathcal{B}} \boldsymbol{N}^{\mathrm{T}} \boldsymbol{F}\, dV + \int_{\partial\mathcal{B}} \boldsymbol{N}^{\mathrm{T}} \boldsymbol{T}\, dA}_{\boldsymbol{F}^{ext}} \tag{24}$$

where $\boldsymbol{T} = [\bar{t}_1 \;\; \bar{t}_2 \;\; \bar{m}_3]^{\mathrm{T}}$ and $\boldsymbol{F} = [\rho g_1 \;\; \rho g_2 \;\; \rho(\boldsymbol{J}\cdot\boldsymbol{c})_3]^{\mathrm{T}}$ are generalized traction and body force vectors, respectively. The non-linear system of equations is solved by a modified implicit-explicit scheme which is originally proposed in Hughes et al. [27] and Prevost [28] to solve single-scale hydro-mechanical transient problems. This solution scheme for DEM-FEM model allows larger time step size compared to explicit scheme and avoids additional computational cost in computing the elasto-plastic tangential stiffness from DEM RVEs in fully implicit scheme. The implicit-explicit predictor-corrector scheme is performed by evaluating a portion of the left hand side forces explicitly using the predicted solution $\tilde{\boldsymbol{d}}$ defined as:

$$\tilde{\boldsymbol{d}} = \boldsymbol{d_n} \tag{25}$$

and by treating the remaining portion implicitly with the solution $\boldsymbol{d_{n+1}}$:

$$\boldsymbol{d_{n+1}} = \tilde{\boldsymbol{d}} + \Delta \boldsymbol{d_{n+1}} \tag{26}$$

The implicit-explicit partition reads,

$$\boldsymbol{F}^{int}_{\mathrm{IMP}}(\boldsymbol{d_{n+1}}) + \boldsymbol{F}^{int}_{\mathrm{EXP}}(\tilde{\boldsymbol{d}}) = \boldsymbol{F^{ext}_{n+1}} \tag{27}$$

To obtain the incremental update of the macroscopic displacement and micropolar rotation from the non-linear system of equations, Newton-Raphson method is employed. As a result, the consistent linearization of the implicit part $\boldsymbol{F}_{\mathrm{IMP}}$ is required. The resulting tangential stiffness matrix depends on what force terms are included in $\boldsymbol{F}^{int}_{\mathrm{IMP}}$.

Since computation of the homogenized $\boldsymbol{K^s}$ from DEM RVEs produces considerable computational cost, in the proposed multi-scale solution scheme, we choose to treat the elastic stiffness $\boldsymbol{K^e}$ implicitly and $\boldsymbol{K^{ep}}$ explicitly. In particular, we assume that the elastic response is linear and isotropic and use a perturbation method to obtain the all the non-polar and micropolar elastic material parameters from the RVEs at the initial step. The resultant operator-split stiffness matrices read,

$$\begin{cases} \boldsymbol{K_T}^{implicit} = \dfrac{\partial \boldsymbol{F}^{int}_{\mathrm{IMP}}}{\partial \boldsymbol{d}} = \boldsymbol{K^e} \\ \boldsymbol{K_T}^{explicit} = -\boldsymbol{K^{ep}} \end{cases} \tag{28}$$

4 NUMERICAL EXAMPLES

The micropolar FEM-DEM model is verified against the problem of stress concentration around a circular hole in a field of uniaxial and uniform tension. Consider a plane stress problem where a circular hole with radius r is streched by an uniform tensile stress field P. Classical elasticity theory states that the stress concentration factor K_c (ratio between the maximum value of tensile stress around the hole and P) is 3. In the realm of microplar theory, however, a reduction of this factor is predicated. The analytical solutions are studied by Mindlin [29] using the couple-stress theory, by Kaloni and Ariman [30] and Neuber [31] using the micropolar

theory, and the solutions are unified by Cowin [32]. These studies conclude that K_c, instead of having the constant value of 3, depends on geometry and material properties, namely the Poisson's ratio ν, the ratio of r to the material characteristic length l and a coupling number N. The micropolar material parameters are explained in details in [33].

The spatial domain, finite element discretization and boundary conditions of the numerical problem are illustrated in Fig. 4. Due to the symmetry of the problem domain, only a quarter of the circular hole is solved. On the two cutting-planes, the normal displacements as well as the rotations are restricted to zero. The circular hole has the radius of $0.05m$ while the patch size is $1m$, ensuring a uniform tension field P applied around the hole. A strongly gradated mesh is used to efficiently capture the stress concentration field around the hole. The DEM sample attached to all Gauss integration points of the finite elements is also shown. The grains with radius of $0.05m$ are arranged in a 5x5 cubic array and a concrete interaction model is used to allow tensile forces between the particles [34]. The DEM sample is initially stress-free and remains in elastic region under the uniaxial tension field.

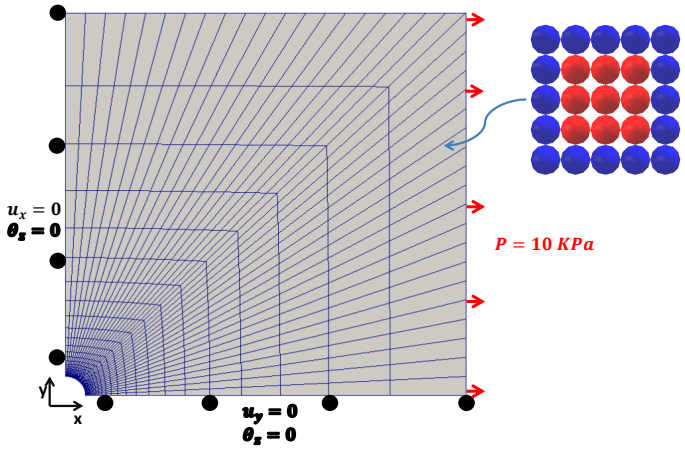

Figure 4: Geometry, mesh, boundary conditions and DEM RVE for stress concentration problem

The material parameters in the context of the micropolar elasticity theory and the values identified from the DEM concrete sample using the perturbation method are recapitulated in Table 1. Note that the internal length l is 0.718 of the grain radius, which is in accordance with the Mindlin's statement that l is about 0.75 of the radius of a sphere when the identical elastic spheres are arranged in a simple cubic array [29].

The Cauchy stress and couple-stress fields around the circular hole given by the micropolar FEM-DEM model are presented in Fig.5. The stress concentration factor $K_c = \max(\sigma_{xx})/P$ is about 2.6, smaller than the value of 3 predicted by the classical continuum theory. The distributions of couple-stress μ_{xz} and μ_{yz} are symmetric about the bisectrix line. The existence of these couple-stresses results in the asymmetry of the Cauchy stress, as illustrated by the field of difference of shear stresses $|\sigma_{xy} - \sigma_{yx}|$ (Fig. 5(c)).

To illustrate the effect of material length scale l on the stress concentration factor, the grain radius of the DEM concrete sample is varied ($r = 0.1m,\ 0.05m,\ 0.01m,\ 0.005m,\ 0.001m$). The length scales l are always 0.718 of the corresponding radius and the Poisson's ratio ν and the coupling number N remain the same values. The stress concentration factor K_c is plotted

Micropolar material parameters (notations in consistent with [33])	Value identified from DEM
Micropolar Young's modulus E_m	$4.802 \times 10^9\ Pa$
Poisson's ratio ν	0.235
Micropolar shear modulus G_m	$2.255 \times 10^9\ Pa$
Shear modulus μ^*	$1.916 \times 10^9\ Pa$
Modulus between anti-symmetric parts κ	$6.783 \times 10^8\ Pa$
Modulus of curvature γ	$1.163 \times 10^7\ N$
Coupling number N ($N = \sqrt{\frac{\kappa}{2(\mu^*+\kappa)}}$)	0.362
Internal length scale l ($l = \sqrt{\frac{\gamma}{2(2\mu^*+\kappa)}}$)	$0.0359m$

Table 1: Micropolar elasticity material parameters in the stress concentration problem

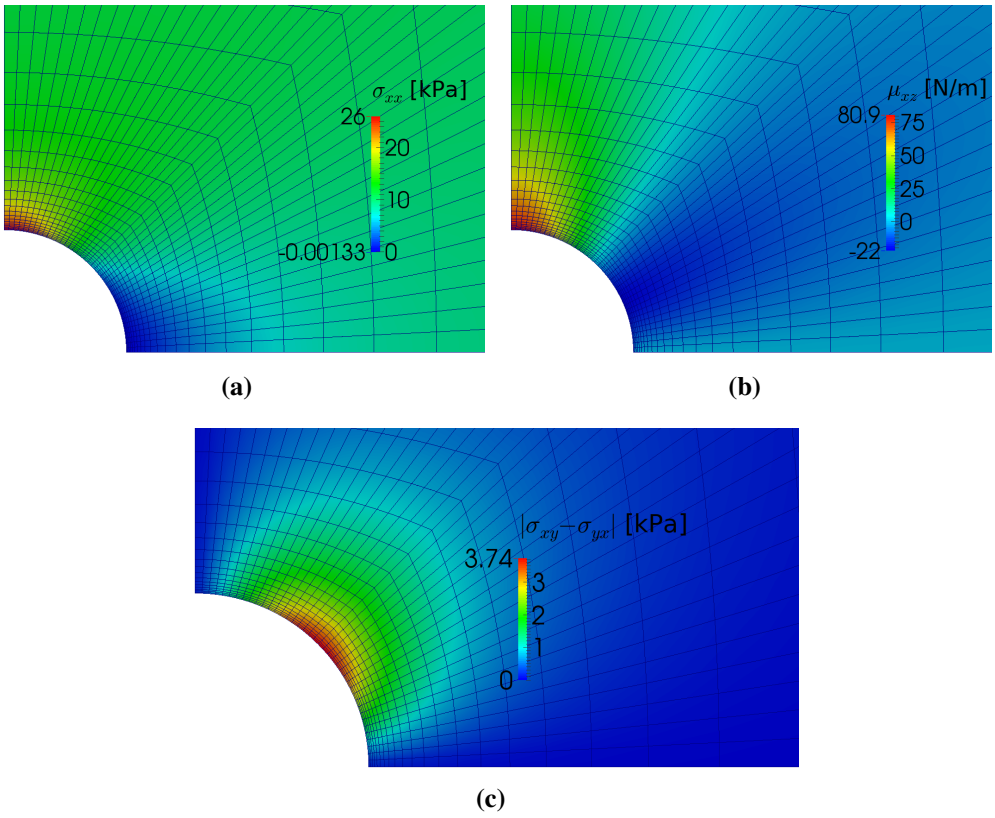

(a) **(b)**

(c)

Figure 5: Stress field around a circular hole under tension.

against the length ratio r/l in Fig. 6. The same variation trend of K_c between the multiscale solution and the analytical solution is observed. This study provides evidence that our multiscale model intrinsically incorporates the internal material length scale.

5 CONCLUSIONS

A new higher-order DEM-FEM model for granular materials is established by incorporating higher-order kinematics and second-order homogenization theory. This work demonstrates the possibility of using grain-scale simulations as a replacement of phenomenological constitutive

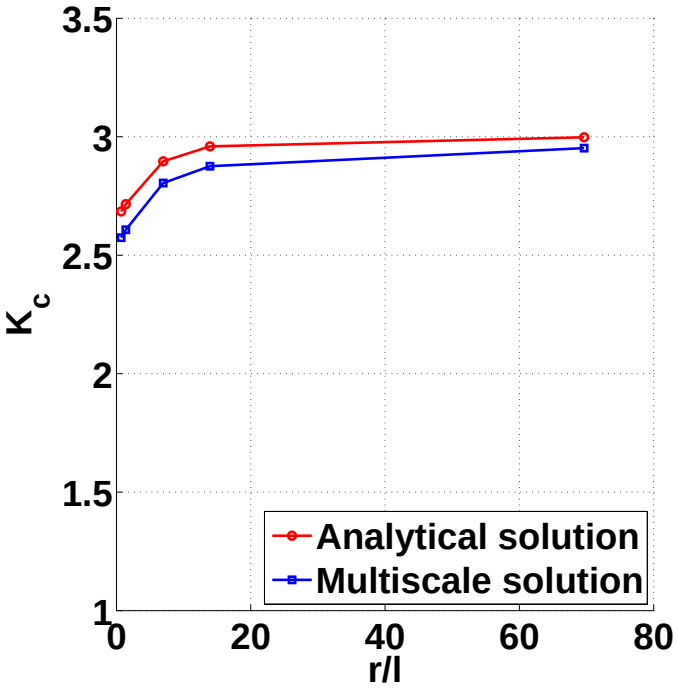

Figure 6: The stress concentration factor K_c as a function of length ratio r/l. Comparison between multiscale model solutions and analytical solutions [32]

law for micropolar continua. The resultant scheme retrieves the characteristic length naturally from the DEM assemblies, without the need to explicitly define one via a nonlocal integral. Another key upshot of the proposed high-order multiscale scheme is that it does not require any additional material parameters other than the one required for DEM. These features greatly simplifies the material identification procedure an allow one to analyze the interplay between evolution of micro-structural attributes and the macroscopic outcome.

6 ACKNOWLEDGMENTS

This research is supported by the Earth Materials and Processes program at the US Army Research Office under grant contract W911NF-14-1-0658 and W911NF-15-1-0581, as well as the Mechanics of Material program at National Science Foundation under grant contract CMMI-1462760 and Provost's Grants Program for Junior Faculty who Contribute to the Diversity Goals of the University at Columbia University. These supports are gratefully acknowledged.

REFERENCES

[1] Kun Wang and WaiChing Sun. Anisotropy of a tensorial bishop's coefficient for wetted granular materials. *Journal of Engineering Mechanics*, 2015. doi: 10.1061/(ASCE)EM.1943-7889.0001005.

[2] Kun Wang and WaiChing Sun. A semi-implicit discrete-continuum coupling method for porous media based on the effective stress principle at finite strain. *Computer Methods in Applied Mechanics and Engineering*, 2016. ISSN 0045-7825. doi: http://dx.doi.org/10.1016/j.cma.2016.02.020.

[3] David L Henann and Ken Kamrin. Continuum modeling of secondary rheology in dense granular materials. *Physical review letters*, 113(17):178001, 2014.

[4] WaiChing Sun, Matthew R Kuhn, and John W Rudnicki. A multiscale dem-lbm analysis on permeability evolutions inside a dilatant shear band. *Acta Geotechnica*, 8(5):465–480, 2013.

[5] WaiChing Sun. A unified method to predict diffuse and localized instabilities in sands. *Geomechanics and Geoengineering*, 8(2):65–75, 2013.

[6] Yang Liu, WaiChing Sun, Zifeng Yuan, and Jacob Fish. A nonlocal multiscale discrete-continuum model for predicting mechanical behavior of granular materials. *International Journal for Numerical Methods in Engineering*, 2015. ISSN 1097-0207. doi: 10.1002/nme.5139.

[7] Matthew R Kuhn, WaiChing Sun, and Qi Wang. Stress-induced anisotropy in granular materials: fabric, stiffness, and permeability. *Acta Geotechnica*, 10(4):399–419, 2015.

[8] John Walter Rudnicki and JR Rice. Conditions for the localization of deformation in pressure-sensitive dilatant materials. *Journal of the Mechanics and Physics of Solids*, 23 (6):371–394, 1975.

[9] WaiChing Sun and Alejandro Mota. A multiscale overlapped coupling formulation for large-deformation strain localization. *Computational Mechanics*, 54(3):803–820, 2014.

[10] WaiChing Sun. A stabilized finite element formulation for monolithic thermo-hydro-mechanical simulations at finite strain. *International Journal for Numerical Methods in Engineering*, 103(11):798–839, 2015.

[11] SeonHong Na and WaiChing Sun. Wave propagation and strain localization in a fully saturated softening porous medium under the non-isothermal conditions. *International Journal for Numerical and Analytical Methods in Geomechanics*, 2016.

[12] Eugène Cosserat and François Cosserat. Théorie des corps déformables. *Paris*, 1909.

[13] A Cemal Eringen and ES Suhubi. Nonlinear theory of simple micro-elastic solidsi. *International Journal of Engineering Science*, 2(2):189–203, 1964.

[14] Masanobu Oda and Kazuyoshi Iwashita. Study on couple stress and shear band development in granular media based on numerical simulation analyses. *International journal of engineering science*, 38(15):1713–1740, 2000.

[15] Wenxiong Huang and Erich Bauer. Numerical investigations of shear localization in a micro-polar hypoplastic material. *International journal for numerical and analytical methods in geomechanics*, 27(4):325–352, 2003.

[16] Jia Lin, Wei Wu, and Ronaldo I Borja. Micropolar hypoplasticity for persistent shear band in heterogeneous granular materials. *Computer Methods in Applied Mechanics and Engineering*, 289:24–43, 2015.

[17] Christian Miehe and Joachim Dettmar. A framework for micro–macro transitions in periodic particle aggregates of granular materials. *Computer Methods in Applied Mechanics and Engineering*, 193(3):225–256, 2004.

[18] N Guo, J Zhao, and WaiChing Sun. Multiscale analysis of shear failure of thick-walled hollow cylinder in dry sand. *Géotechnique Letters*, 6(1):1–6, 2016.

[19] Yang Liu, WaiChing Sun, and Jacob Fish. Determining material parameters for critical state plasticity models based on multilevel extended digital database. *Journal of Applied Mechanics*, 88(1), 2016.

[20] Jacob Bear and Yehuda Bachmat. *Introduction to modeling of transport phenomena in porous media*, volume 4. Springer Science & Business Media, 1990.

[21] Sia Nemat-Nasser and Muneo Hori. *Micromechanics: overall properties of heterogeneous materials*. Elsevier, 2013.

[22] I Vardoulakis. Lecture notes on cosserat continuum mechanics with application to the mechanics of granular media. In *3rd National Meeting on Generalized Continuum Theories and Applications, Thessaloniki, Greece*, 2009.

[23] Ragnar Larsson and Stefan Diebels. A second-order homogenization procedure for multiscale analysis based on micropolar kinematics. *International journal for numerical methods in engineering*, 69(12):2485–2512, 2007.

[24] J Christoffersen, MM Mehrabadi, and S Nemat-Nasser. A micromechanical description of granular material behavior. *Journal of Applied Mechanics*, 48(2):339–344, 1981.

[25] Katalin Bagi. Stress and strain in granular assemblies. *Mechanics of materials*, 22(3): 165–177, 1996.

[26] JP Bardet and I Vardoulakis. The asymmetry of stress in granular media. *International Journal of Solids and Structures*, 38(2):353–367, 2001.

[27] Thomas JR Hughes, Karl S Pister, and Robert L Taylor. Implicit-explicit finite elements in nonlinear transient analysis. *Computer Methods in Applied Mechanics and Engineering*, 17:159–182, 1979.

[28] Jean H Prevost. Implicit-explicit schemes for nonlinear consolidation. *Computer Methods in Applied Mechanics and Engineering*, 39(2):225–239, 1983.

[29] RD Mindlin. Influence of couple-stresses on stress concentrations. *Experimental Mechanics*, 3(1):1–7, 1963.

[30] Puran N Kaloni and Teoman Ariman. Stress concentration effects in micropolar elasticity. *Zeitschrift für angewandte Mathematik und Physik ZAMP*, 18(1):136–141, 1967.

[31] H Neuber. On the general solution of linear-elastic problems in isotropic and anisotropic cosserat continua. In *Applied Mechanics*, pages 153–158. Springer, 1966.

[32] Stephen C Cowin. An incorrect inequality in micropolar elasticity theory. *Zeitschrift für Angewandte Mathematik und Physik (ZAMP)*, 21(3):494–497, 1970.

[33] S Bauer, M Schäfer, P Grammenoudis, and Ch Tsakmakis. Three-dimensional finite elements for large deformation micropolar elasticity. *Computer Methods in Applied Mechanics and Engineering*, 199(41):2643–2654, 2010.

[34] Václav Šmilauer. *Cohesive particle model using the discrete element method on the yade platform*. PhD thesis, Université de Grenoble; Czech Technical University in Prague (http://www. cvut. cz), 2010.